PCCP

Accepted Manuscript




ROYAL SOCIETY OF CHEMISTRY

www.rsc.org/pccp

# FLUORESCENCE AND FÖRSTER RESONANCE ENERGY TRANSFER INVESTIGATIONS ON DNA OLIGONUCLEOTIDE AND PAMAM DENDRIMER PACKING INTERACTIONS IN DENDRIPLEXES

**Hema Kumari Alajangi and Deenan Santhiya***

**Delhi Technological University, Department of Applied Chemistry and Polymer Technology, Bawana Road, Delhi-110 042, India**

***To whom corresponding should be addressed E-mail: deenan.santhiya@dce.ac.in**

**ABSTRACT**

Considering the importance of short oligonucleotide packing in dendriplex mediated gene delivery, a direct insight on the 14mer oligonucleotide and dendrimer interactions was focused using fluorescence and FRET techniques. Fluorometric titrations of various fluorophore tagged oligonucleotides with first three PAMAM dendrimer generations showed a decrease in fluorescence intensity with two break points namely $Z^1_{\pm}$ and $Z^2_{\pm}$ for each titration. The first break point for each dendrimer was identical with the neutralization point observed by basic biophysical studies for the corresponding dendrimer generations. Additionally, FRET studies on dual tagged oligonucleotide ($D_{FT}$) molecules revealed a third break point at the charge ratio ($Z^3_{\pm}$) where there was the highest fluorescence energy transfer from the donor to the acceptor fluorophores. Altogether, the dendriplex formation was considered to take place via three steps with increase in the dendrimer concentration, where initially there was monomeric complexation at neutralization point ($Z^1_{\pm}$) followed by a loosely held molecular aggregation of the dendrimer ($Z^2_{\pm}$). At final step, dendrimer molecular aggregates were held tight for the closest possible packing of the oligonucleotide molecules onto their surface. The effective molecular packing is identified by the highest FRET intensity for the dendrimer of generation two at the charge ratio 0.34 ($Z_{\pm}$).

**Keywords**: FRET, fluorometric titration, DNA-PAMAM interaction, Non-viral gene delivery

## 1. INTRODUCTION

In recent years, therapeutic gene silencing has attracted a numerous researchers for treating a variety of diseases including viral infections, cancers, myopathies and neurodegenerative diseases by regulating genes due to its potency, selectivity and versatility. Interestingly, gene silencing activity is currently being researched by delivering short synthetic oligonucleotides, such as antisenses, siRNAs and miRNA to control the expression of a specific target gene by inhibiting the corresponding mRNA function without influencing genomic DNA.[1-6] Such an attractive therapeutic strategy is expected to overcome several critical hurdles including off-target effects, toxicity due to saturation of the endogenous RNAi functions, limited duration of silencing, and ineffective targeted delivery before its widespread clinical adoption.[5] In order to overcome these clinical hurdles in gene silencing activity, the use of 21-23 base-pared siRNA is considered to be one of the most promising tool due to its high potency and minimum off-target interaction.[7] Even though, the successful delivery of siRNA molecule with high efficiency still faces challenges for *in vivo* delivery due to its low resistance against enzymatic degradation, limited translocation across the cell membrane and a substantial liver clearance.[8] Apart from these, due to the relatively small size of these oligonucleotides, the requirement for vectors designed for their *in vitro* or *in vivo* delivery is observed to be more stringent than the delivery of long DNA.[9]

However, a numerous non-viral cationic molecules such as liposomes and cationic polymers including poly(L-lysine), poly(amidoamine) (PAMAM) dendrimers, poly(alkylcyanoacrylate) nanoparticles and poly(ethylene imine) are observed to be successful for the siRNA delivery into the target cells.[10-14] These cationic carriers are well known to interact electrostatically with the anionic nucleic acid molecules by forming nano-sized siRNA-polymer complexes which can protect nucleic acids from non-specific interactions and enzymatic degradation in the systemic circulation.[15]Among the other cationic vectors, dendrimers are considered to be interesting polymeric gene carriers in non-viral gene therapy due to their synthetically tunable molecular structure, size, surface charge as well as functionality. More importantly, highly definable mono-dispersed population is observed in dendrimers due to their uniform size and distribution of surface charge for efficient delivery of therapeutic genes. Further, these cationic macromolecular vectors without as well as with varied core/branching structures are shown to form stable complexes with nucleic acids by protecting them from

nucleases and are used extensively for the *in vitro* delivery of plasmid DNA as well as antisense oligonucleotides and siRNA in various cell lines.[16-19] For example, PAMAM-DNA, poly(ethyleneglycol)-modified PAMAM-DNA, PAMAM-PEG-PAMAM-DNA, PPI-DNA and PEI-DNA interactions reveal a numerous formulations for dendrimer-DNA polyplexes[18,19] and a few reports also indicating usefulness of functionalized PAMAM dendrimers as *in vivo* gene delivery vehicles into kidney [20] and brain [21] tissue of mice. Even though PAMAM dendrimers of higher generations especially above 4 are shown to be better gene carriers in spite of their cytotoxicity[18, 19] recently there are few interesting studies highlighting the importance of lower generation dendrimers. For example, the lower generation dendrimers G2 and G4 are shown as potential POPC (palmitoyloleoylphosphatidylcholine) model biomembrane transfection mediators.[22] Interestingly, siRNA/G1 PAMAM dendriplex is found to decrease both p42-MAPK mRNA and protein levels and could potentiate the antitumoral activity of anticancer drugs[23] and the lower PAMAM dendrimer generation 2 is proved to be superior to those of G4 in skin penetration.[24]

Most of these dendrimer studies also reveal that there is a need of controlled and triggered nucleic acid delivery from the carrier complex by analyzing structure-property relationships of dendrimer-oligonucletide delivery systems for successful gene and gene silencing therapies. For example, Norden and co-workers[25] demonstrated how the condensation degree of plasmid DNA-poly(amidoamine) dendrimer of generation 5 complex affects enzyme accessibility and gene expression. Interestingly here, a high-density dendriplex was identified to turn off gene expression, whereas uncondensed DNA behavior was observed in the case of low-density dendriplex. Using fluorescence lifetimes and time-resolved spectra, Yliperttula *et al*[26] showed easy release of DNA from DNA-poly (ethylenimine) (PEI) complex to the right intracellular site was possible due to their different binding energies. In contrast, because of only one DNA conformation in the poly (L-lysine) (PLL) based polyplexes, DNA disintegration was found to be difficult.

Unlike plasmid DNA, rigid rod-structured therapeutic short oligonucleotides (antisenses, siRNAs, and miRNA) do not compact efficiently when complexed with a vector and leads to incomplete encapsulation and the formation of undesirably large complexes.[27,28] Consequently, the usual cationic polymers proven effective for gene delivery are not necessarily optimal for these short nucleic acids.[29] Eventhough, recent literature highlights well about siRNA binding

capacity of dendrimers indirectly through techniques like dynamic light scattering (DLS), nanoparticle tracking analysis (NTA), atomic force microscopy (AFM), Transmission electron microscopy (TEM), poly(acrylamide) gel electrophoresis, and ethidium bromide displacement assay,[30,31,32] most direct insights into dendrimer and short oligonucleotide packing interaction in the dendriplexes are scare and still need to be explored with more advanced tools. With this consideration, present study involves synthetic 14mer oligonucleotide interaction with Poly (amidoamine) (PAMAM) dendrimers of generations one, two and three (G1, G2 and G3) using fluorescence and Fröster resonance energy transfer (FRET) methods. FRET is widely used technique to quantify molecular dynamics in protein-protein interaction, protein-DNA interactions and protein conformational changes. Using FRET technique, three steps in oligonucleotide-CTAB interactions were investigated by us[33] using labelled oligonucleotide strand I with a donor fluorophore and the other with an acceptor fluorophore. Here, the effective accommodation of oligonucleotide around the micellar aggregation of surfactant molecule is interestingly revealed by predominant fluorescence emission of the acceptor molecule due to intermolecular FRET from donor to acceptor. In this investigation we seek to explore dendrimer-short oligonucleic acid packing interactions as nano-complexes for gene silencing applications by FRET technique. Required fluorometric experiments were carried out as follows: synthetic oligonucleotide of 14 base pair was tagged at 5′ with fluorescein (strand I) as well as with tetramethylrhodamine (TAMRA) (strand II) and fluorometric titrations were performed with PAMAM dendrimer of first three generations. Similarly, fluorometric titrations were also carried out for oligonucleotides 5′-tagged with either fluorescein or TAMRA. The oligonucleotide-dendrimer interaction was also investigated by ethidium bromide exclusion and gel electrophoresis studies for first three generations.

## 2. MATERIALS AND METHODS

**Materials.** PAMAM (starburst) dendrimer of generation one, two and three (G1, G2 & G3) of highest purity (>99%) were obtained from Sigma-Aldrich. Chemical structure of one of the representative PAMAM dendrimer, G1, is shown in Figure 1 along with a schematic representation of the first three dendrimer generations. These dendrimers can be named appropriately following the short hand nomenclature introduced by Tomalia *et al*.[34] Accordingly, the nomenclature for the three PAMAM dendrimers will be as follows - (i) G1: [Core:

ethylenediamine]; (4→2); *dendri*-{poly(amidoamine)-($NH_2$)8}; (G=1) dendrimer (ii) G2: [Core: ethylenediamine]; (4→2); *dendri*-{poly(amidoamine)-($NH_2$)16}; (G=2) dendrimer (ii) G3: [Core: ethylenediamine]; (4→2); *dendri*-{poly(amidoamine)-($NH_2$)32}; (G=3) dendrimer. Unlabeled 14mer DNA oligonucleotide of strand I (5'-GATGTTCACTCCAG-3') and strand II (5'-CTGGAGTGAACATC-3') were procured from SBS-Genetech. In addition to these, fluorescein tagged with 5' end of the 14mer strand I oligonucleotide (5'-GATGTTCACTCCAG-3') and its complementary strand II oligonucleotide (5'-CTGGAGTGAACATC-3') tagged with tetramethylrhodamine (TAMRA) at the 5' end were also supplied by SBS-Genetech. As per the manufacturer the GC content of the oligonucleotide was reported to be 50%. The concentration of unlabeled oligonucleotide was calculated by extrapolation of tabulated values of the monomer bases at 25 °C [35, 36] whereas, concentrations of labelled strands were determined based on optical density (OD) values provided by the manufacturer.

**Preparation of various duplexes with different combinations of oligonucleotides.** In order to obtain untagged ($D_0$) duplex, equimolar concentrations of both the unlabeled oligonucleotide strands were mixed and the mixture was heated to 95°C for 10 minutes and cooled to room temperature for 4-6 h. Similarly, labeled duplexes were also prepared. To prepare 5′-fluorescein labeled duplex ($D_F$), 5′-fluorescein tagged strand I was mixed with untagged strand II. 5′-TAMRA tagged duplex ($D_T$) was made by mixing unlabeled strand I and 5′ -TAMRA tagged strand II. Dual tagged oligonucleotide ($D_{FT}$) was obtained by mixing 5′ fluorescein tagged strand I and 5′-TAMRA labeled strand II. All experiments were done in 10 mM sodium phosphate buffer, pH 7.0. Here 1 $\mu$M 14mer oligonucleotide is equivalent to a 26 $\mu$M (as 14mer single strand oligonucleotides contain 13 phosphate groups) phosphate unit. Stock solutions of PAMAM dendrimer of 1, 2 and 3 generations were prepared by dissolving the required amount of dendrimer of desired generation in a known volume of phosphate buffer solution (18.2 mg/10 mL) and the corresponding concentrations were determined gravimetrically. In the entire text, in order to study the PAMAM dendrimer to DNA interaction, the resulting DNA-Dendrimer complex has been quantified by charge ratio ($Z_{+/-}$) which expresses the ratio (N/P) of concentration of cationic charges on dendrimer (N) to DNA phosphate groups (P). All the other reagents used were of AR grade purity. Milli-Q water was used for all the experiments.

**Gel Electrophoresis Studies.** The electrophoretic mobilities of PAMAM dendrimer of generations 1, 2 & 3 and untagged oligonucleotide (14 mer) complexes at various charge ratios $Z_{(+/-)}$ were determined by using 15% native-PAGE. Gel electrophoresis experiments were carried out in a buffer consisting of 45 mM Tris-borate and 1 mM EDTA at pH 8.0. In these studies, in order to prepare oligonucleotide-dendrimer complex of required charge ratio, 1 $\mu$M concentration of oligonucleotide (equivalent to 26 $\mu$M phosphate unit) was mixed with various concentrations of the desired dendrimer generations (1, 2 & 3) solution and incubated for 30 min. Polyacrylamide gels were run at 120 V for 4 h at 4 °C using the oligonucleotide-dendrimer complexes of various charge ratios. Further, the corresponding dendriplex bands were visualized under UV illumination after staining the gels with ethidium bromide for 30 min at room temperature.

**UV-melting studies.** UV-melting experiments were performed using Cary 100 concentration UV-visible spectrophotometer with temperature controller on various duplexes. Melting experiments were carried out by heating 1 $\mu$M concentration of unlabelled ($D_0$), tagged with 5′-fluorescein ($D_F$), labelled with 5′-TAMRA ($D_T$) and tagged with 5′-fluorescein as well as 5′-TAMRA ($D_{FT}$) from 20 to 95°C at a scanning rate of 1.0 °C/min in a 1000 µL cuvette. The melting profiles of the oligonucleotides were recorded by monitoring the absorbance of the complexes at 260 nm as a function of temperature. Transition temperatures ($T_m$) were calculated from the melting curves and revealed that their $T_m$ values were in the range of 33 to 37 °C (data not shown).

**Circular Dichroism studies.** CD spectra of the untagged oligonucleotide ($D_0$) were recorded using a Jasco spectropolarimeter (model 715) equipped with a peltier thermostat controlled cell holder at 20 °C and a cuvette with a path length of 1 cm. The CD spectra of untagged duplex were recorded between 220 and 325 nm in the absence and presence of the desired dendrimer generations of 1, 2 & 3 in 10 mM sodium phosphate buffer, pH 7.0. Various amounts (maximum of 30 $\mu$L) of the polymer stock solutions (mostly 5 mM dendrimer generations of 1, 2 & 3) were added to 5 $\mu$M oligonucleotide solutions. The complexes were incubated for 10 min before each CD measurement. The titration of the dendrimer was terminated, when significant change was not observed in the corresponding CD signal. Once again, the dilution of oligonucleotide was maintained within 10%.

**Ethidium bromide exclusion studies.** In order to understand dendrimer based short oligonucleotide delivery system, ethidium bromide (EB) exclusion studies were carried out as follows: Fluorescence spectra of oligonucleotide-EB complexes were recorded in the absence and presence of the desired generation of PAMAM dendrimer from 500 to 700 nm, at an excitation wavelength ($\lambda_{ex}$) of 480 nm using a spectrofluorometer (JobinYvon FluoroMax 3) with a peltier thermostat. A 14 μM concentration of EB was mixed with a 1 μM concentration of oligonucleotide solutions (1EB:1base pair) in 10 mM sodium phosphate buffer at pH 7.0 and equilibrated for 10 min at 20 °C. For these experiments, a stock EB solution was prepared by dissolving 1.97 mg of EB in 1000 $\mu$L of water, and the corresponding stock concentration was determined using a Cary 100 concentration UV-visible spectrophotometer assuming molar extinction coefficient 5600 L $mol^{-1}$ $cm^{-1}$ at 480 nm.[37] 300 μL of this oligonucleotide-EB mixture was taken in a fluorescence cuvette, and increasing amounts of the cationic polymer of the required concentration were added into the mixture. After each addition of the polymer, the content of the fluorescence cuvette was incubated for 10 min before recording each spectrum. The concentrations of dendrimer stock solutions were prepared in such a way that the maximum dilution of oligonucleotide-EB complex was maintained well within 10% due to the dendrimer addition. The dilution factors considered for the calculation were of final charge ratios. The percentage of EB release from the DNA upon the interaction with the cationic polymers was calculated according to: $(I_0\text{-}I)/(I_0\text{-}I_{EB})\times100$, where $I_0$ and $I_{EB}$ are the fluorescence intensities of free and oligonucleotide-bound EB, and I is the fluorescence intensity in the presence of different amounts of dendrimer.

**Fluorescence and FRET Studies.** The fluorescence spectra of dual labeled oligonucleotide ($D_{FT}$) were recorded by following our earlier procedure:[33] Initially, fluorescence spectra of a 1 $\mu$M concentration of fluorescein tagged strand I were recorded from 500 to 700 nm, at an excitation wavelength ($\lambda_{ex}$) of 490 nm and at temperature 15 °C using a spectrofluorometer (JobinYvonFluoroMax 3) with a Peltier thermostat. Then the strand I was mixed with the required amount of TAMRA tagged strand II to maintain equimolar concentration as 1 $\mu$M in 300 $\mu$L. The corresponding duplex was prepared in the fluorescence cuvette by heat-cool treatment using a Peltier thermostat, and the spectrum was recorded. The required amount of desired generation of PAMAM dendrimer was added to the duplex. After each addition, the resulting oligonucleotide-dendrimer complexes were equilibrated for 10 min

before recording of each fluorescence spectrum. The addition of the cationic polymer was terminated when the corresponding maximum intensity ($I_{max}$) of the fluorescence signal for the dual labeled duplex became saturated. Similarly, fluorescence spectra of oligonucleotides containing fluorescein labeled strand I and unlabeled strand II ($D_F$) as well as untagged strand I and TAMRA tagged strand II ($D_T$) were recorded both in the absence and in the presence of dendrimer at an excitation wavelength ($\lambda_{ex}$) of 490 and 520 nm respectively at 15 °C. In all the experiments, the stock concentration of dendrimer generations – 1, 2 & 3 solutions was chosen such that the maximum dilution of oligonucleotide- dendrimer complex was maintained well within 10% due to the addition of the cationic polymer. The polymer as well as oligonucleotide concentrations were calculated by including the dilution factors, which were also maintained within 10% of the initial volume (300 $\mu$L).

## 3. RESULTS AND DISCUSSION

**Gel electrophoresis studies.** The interaction between therapeutic nucleic acid and cationic vector can be visualized by gel electrophoresis for the development of non-viral gene delivery system. Due to the association of positively charged cationic vector with the negatively charged nucleic acid, there exists partial or complete neutralization of the negative charges of the nucleic acid. The migration of such partially or completely neutralised DNA is either slow down or completely hindered through the gel.[35] Gel electrophoresis studies were carried out on the 14mer before and after interaction with PAMAM dendrimer of three generations G1, G2 and G3 and the results are displayed in Figure 2. First and second wells of all the three PAGEs correspond to the migration of 10 bp molecular weight marker and free DNA respectively. Whereas, subsequent wells of the PAGE represent the migration of oligonucleotide-dendrimer complexes at increasing PAMAM dendrimer to the 14mer oligonucleotide charge ratio (from $Z_{\pm}$ = 0.3 to $Z_{\pm}$ = 2.7). In Figure 2a, migration of oligonucleotide is seen upto dendrimer G1 to oligonucleotide charge ratio 0.3. It is pertinent to mention that smearing and reduction in the intensity of the band corresponding to the DNA-G1 complex at charge ratio 0.3 is observed compared to free DNA ($Z_{\pm}$ = 0). Further, DNA migration is completely not visible from the charge ratio 0.6 to 2.7 ($Z_{\pm}$). The observation in the case of Fig. 2a suggests interactions between the 14 mer DNA and the corresponding dendrimer are highly cooperative. There exists a coexistence of both partially as well as completely neutralised oligonucleotide in the case of

G1upto $Z_{\pm}$ = 0.3 and thereafter it becomes completely saturated. In the presence of dendrimer of generation 2 (Fig. 2b), a very short DNA smearing is observed up to the charge ratio $Z_{\pm}$ = 0.6 indicating the existence of partially neutralised oligonucleotide in trace amounts. Interestingly, DNA migration is retarded completely for oligonucleotide-G2 as well as oligonucleotide-G3 systems from the charge ratio $Z_{\pm}$ = 1.2 to 2.7 (Fig. 2b) and $Z_{\pm}$ = 0.3 to 2.7 (Fig. 2c) respectively and the corresponding wells of the gel are found to contain perturbed DNA-dendrimer complex for generation two (from $Z_{\pm}$ = 0.6 to 2.7) and three (from $Z_{\pm}$ = 0.3 to 2.7). Such disappearance of the DNA band at lower charge ratios ($Z_{\pm}$ = 0.3) is suggestive of effective neutralization of the 14mer with dendrimer of generation two (G2) and three (G3) compare to G1 due to the increase in positive surface charge density of the PAMAM dendrimer with increase in generation. In the presence of G2 and G3, prominently visible retarded DNA at the wells indicates the accessibility of the stain inside the polyplex, which may also reveal inability of the shortest oligonucleotide to undergo compaction.

**CD Measurements:** Based on CD measurements, minute conformational changes in the double helix of 14mer oligonucleotide can be followed due to the possible binding interactions with PAMAM dendrimer of various generations. The CD spectra of 5 μM concentration of oligonucleotide and its complexes with PAMAM dendrimer of generation one (G1) at various charge ratios are depicted in Fig. 3a. From the figure, the observed positive peak at 274 nm and negative peak at 240 nm for the free 14mer oligonucleotide confirms its typical B form signature of double helical DNA and is in good agreement with the literature.[39] Interestingly, the intensity of positive as well as negative CD signals decrease gradually upon successive increase in polymer-oligonucleotide charge ratio, but not disappeared. The appearance of CD signals even at the highest polymer to oligonucleotide charge ratio indicates the existence of the oligonucleotide in B form. The observed incomplete encapsulation of 14mer oligonucleotide by the dendrimer is also evidenced by many researchers especially in the case of rigid rod-structured therapeutic short oligonucleotides in the vicinity of cationic vectors.[28-30] The reduction in amplitude of both the CD signals at 274 and 240 nm are in good agreement with the literature[39] and attributed to the electrostatic attraction of the 14mer oligonucleotide on the dendrimer of generation one. Additionally, there was no major shifting observed in the 14mer CD signals after interaction with the dendrimer. Similarly, in the presence of PAMAM dendrimer of generation two (G2) (Fig. 3b) and three (G3) (Fig. 3c), the intensity of positive as well as negative peaks of CD spectrum

decreases with increase in polymer concentration. In comparison, extend of reduction in the intensity of CD signals increase with increase in the generation of dendrimer for similar dendrimer to oligonucleotide charge ratio. Such increase in the reduction clearly indicates stronger electrostatic interaction of DNA with increase in the positive surface charge density of dendrimer. As observed with dendrimer generation one, the CD signals are not collapsed in the presence of the polymer generation two and three, even at the highest charge ratio used. Figure 3d summarises the changes observed to CD signals at 274 nm in the presence of dendrimers G1, G2 and G3 at various charge ratios normalised at 1. A saturation in CD signals was observed at charge ratios 0.30, 0.18 and 0.12 for the polymer generation one, two and three respectively. Based on the observations of CD signal saturation, it can be concluded that only a lesser amount of the dendrimer is sufficient to neutralise the 14mer with increase in dendrimer generation due to the increase in its positive charge density with generation. The reported CD saturation results are in good agreement with gel electrophoresis studies (Fig. 2) in which disappearance of DNA bands are observed after the charge ratio ($Z_{\pm}$) 0.3 for G1 and 0 for G2 and G3.

**Ethidium bromide exclusion studies.** In these studies, ethidium bromide, a planar aromatic dye is used as a fluorescence spectroscopic probe to determine relative affinities of PAMAM dendrimer of various generations (G1, G2 and G3) for the oligonucleotide. EB is well known to show a striking increase in fluorescence efficiency by intercalating between the base pairs of double helix DNA and is used extensively to probe DNA-cationic vector interactions in the development of non-viral gene delivery systems. The competition between the EB and the cationic co-solutes can be followed by determining quenching in fluorescence intensity of DNA-EB complex.[40,41] Figures 4a-4c at the left panel portray fluorescence emission spectra of free EB solution, oligonucleotide intercalated with EB and oligonucleotide-PAMAM dendrimer complex of generation one (G1), two (G2) and three (G3) respectively. Traces 1 and 2 in each figure represent the spectra due to the free and bound EB with the 14 mer. The observed fluorescence quenching of DNA-EB complex with increase in dendrimer concentration is represented by the down arrow. For all the three dendrimer generations, a reduction in fluorescence intensity with increase in the concentration of dendrimer was observed initially followed by a small negligible fluorescence decrease at higher concentration. The amount of EB that was efficiently released from the DNA molecule by the addition of cationic dendrimer was clearly different for various dendrimer generations used. The percentage EB released from the oligonucleotide with respect

to dendrimer-DNA charge ratio (Figure not shown) has also been carried out. For dendrimer generation one, EB release was initially gradual upto the charge ratio ($Z_{\pm}$) 0.3, thereafter became very slow and finally 90% of EB was released from the oligonucleotide at the highest charge ratio studied ($Z_{\pm}$ = 1). Similar EB release behaviour was also observed for PAMAM dendrimer of generation two and three. Interestingly, the break between gradual as well as slow release of EB from the 14mer was also seen at $Z_{\pm}$ = 0.2 and $Z_{\pm}$= 0.1 for G2 and G3 respectively. Both the dendrimer generations two and three were able to release 90% as well as almost 100% EB from the DNA at the highest dendrimer-DNA charge ratio ($Z_{\pm}$= 1).

EB titration curves of the 14mer–dendrimer system for first three generations (G1, G2 and G3) are portrayed in Figure 4 (a-c, right panel). In general for all the three polymers, quenching of EB fluorescence increases sharply with increase in the cationic polymer concentration and attains an imperfect plateau like region, where negligible quenching was observed. The polymer to the oligonucleotides charge ratio at the onset of the plateau like region is considered as the saturation point for the oligonucleotides by the dendrimer. Further addition of the dendrimer to the solution may bind in a minimal amount to the oligonucleotide and therefore, may exclude EB feebly from oligonucleotides. The region below the saturation point represents the coexistence region of unsaturated dendrimer and the saturated oligonucleotide. It is pertinent to mention that the interaction strength of the first three dendrimer generations (G1, G2, G3) with the oligonucleotide can be represented by the observed saturation point.[39] From the figure, it is evidenced that with increase in dendrimer generation, the dendrimer to the 14mer charge ratio value at the saturation point decreases due to the corresponding rise in their surface charge. For example, the observed breaks for the first three generation of PAMAM dendrimers (G1, G2 and G3) at the onset of the plateau like region are 0.30 (Figure 4a, right panel), 0.20 (Figure 4b, right panel) and 0.07(Figure 4c, right panel) respectively for 1μm oligonucleotide concentration indicated by down arrows. More interestingly, as observed in gel electrophoresis as well as CD experiments, the resulting saturation points from the EB titration curves of G1 and G2 are in good agreement with each other, whereas, in the case of G3 it is more or less same. In these EB titration curves of the oligonucleotide-dendrimer system, the appearance of imperfect plateau region is mostly due to the high charge density of the dendrimer surface in combination with the stiffness of the 14mer helix. As discussed by various researchers,[25,30,33] when a dendrimer molecule is bound to the DNA, the helix cannot bend around it since it is too rigid.

Therefore, the rigid rod like single loop oligonucleotide can occupy only a little portion of the dendrimer. The other unoccupied charged sites of the dendrimer provide a high concentration of positive charges and readily attract a second DNA molecule. As the concentration of dendrimer increases, there may be slight rearrangement of the 14mer molecules on the DNA surface due to the existence of high concentration of unsaturated positive charges on the dendrimer surface and consequent feeble EB exclusion. It is also noteworthy that the observed plateau like region in the EB titration curve for dendrimer generation three (Figure 4c, right panel) is more imperfect due to its higher positive surface charge density compared to G1 and G2.

**Fluorescence studies.** Figure 5a at the left panel portrays fluorescence emission spectra of the 14mer duplex containing 5′-fluorescein tagged strand I and untagged strand II ($D_F$) before and after interaction with increasing concentration of PAMAM dendrimer G1. The free oligonucleotides shows emission maximum at 521 nm upon excitation at 490 nm. The 5′-tagged fluorescein of the duplex shows a decrease in the intensity of fluorescence with increase in dendrimer G1 concentration. It is also noteworthy that the fluorescence emission intensity of $D_F$ shows hardly any change after a particular concentration of G1. Such reported increase in the reduction of the duplex ($D_F$) fluorescence intensity with increasing dendrimer concentration is an indicative of micro environmental change around the fluorescein molecule present in the dendrimer G1-duplex ($D_F$) system. Additionally, the observed unaltered fluorescence emission intensity of $D_F$ at a higher G1 concentration is due to the burial of the fluorescein molecule within the cationic polymer assembly evidencing an attainment of saturation. Interestingly, the observed shift in the emission maxima of 5′-fluorescein to higher wavelength (red shift) for each addition of increasing dendrimer concentration indicates the formation of hydrophobic assemblies of the polymer. The fluorescence emission spectra of oligonucleotide ($D_F$) in the absence and presence of G2 (Fig. 5b, left panel) and G3 (Fig. 5c, left panel) show a similar behavior as observed in the case of the duplex ($D_F$)-dendrimer of generation one (G1) system (Fig. 5a, left panel). In addition to this, it is also noteworthy that the observed red shift in the emission maxima of 5′-fluorescein in the presence of the polymer increases with increase in polymer generation probably due to the increase in their size.

The interaction between the oligonucleotide ($D_T$) containing unlabelled strand I as well as 5′-TAMRA labeled strand II and PAMAM dendrimer of generation one (G1) is shown in Fig. 5a at right panel. In the absence of G1, the fluorescence emission maximum of the 5′-TAMRA

tagged duplex was detected at 582 nm upon excitation at 520 nm. As observed in the case of the duplex $D_F$-G1 system (Fig. 5a, right panel) here again, the fluorescence intensity of 5′-TAMRA tagged oligonucleotide ($D_T$) decreases with increase in the concentration of the dendrimer of generation one (G1) indicating micro environmental changes around the fluorophore due to the oligonucleotide-dendrimer interaction. It is worthwhile to mention that a slight blue shift was observed in the intensity maxima of the duplex ($D_T$) for each increase in dendrimer G1 concentration addition. The behavior of the 5′-TAMRA tagged oligonucleotide in the presence of G2 (Fig, 5b, right panel) and G3 (Fig. 5c, right panel) was observed to be as similar as $D_T$-PAMAM G1 system. In the presence of dendrimer, the observed red as well as blue shift in the fluorescence emission maximum of $D_F$-PAMAM (Fig. 5, left panel) as well as $D_T$-PAMAM (Fig. 5, right panel) systems respectively may be interpreted to the change from polar to non-polar environment around the corresponding fluorophores due to the 14mer and dendrimer complexation. The interesting opposite behavior of the two fluorophores 5′-TAMRA (blue shift) and 5′-fluorescein (red shift) was tested by obtaining emission spectra of these free fluorophores in three different solvents, namely, water, methanol as well as hexane and discussed previously by us.[33] In the case of fluorescein, emission maxima were 518, 521, and 524 nm whereas, in the case of TAMRA, emission maxima were 572, 566, and 557 nm in water, methanol and hexane respectively.[33]

Figure 6 (left panel) portrays fluorescence emission spectra of the dually tagged oligonucleotide ($D_{FT}$) by fluorescein and TAMRA at 5′ ends of its strand I and strand II respectively in the absence and presence of the dendrimer of three generations (G1, G2 and G3). From the figure it is evident that two emission maxima are reported for the oligonucleotide ($D_{FT}$) in the absence of dendrimer of all generations under study. These fluorescence emission maxima were observed as expected one each at 520 and 575 nm corresponding to donor fluorescein and acceptor TAMRA emissions upon excitation at 490 nm respectively. The fluorescence emission intensities decrease in general for donor as well as acceptor for all three generations of PAMAM dendrimer up to certain level of concentration increase. A striking increase in the emission intensity of TAMRA at higher polymer concentration was seen especially for the dendrimer generations G2 (Fig. 6b, left panel) and G3 (Fig. 6c, left panel). On the contrary, similar raise in the emission intensity of TAMRA at higher concentrations is not very much obvious for the polymer generation one (G1)

(Fig. 6a, left panel). Corresponding decrease in the emission intensity of the donor fluorescein for all the generations are reported very moderately in Fig. 6 (left panel). Such changes observed in the emission maxima of fluorescein of the dual tagged oligonucleotide are evidencing only very small amount of resonance energy transfer from donor to the acceptor fluorophore.

In order to bring out the minute differences in the fluorescence energy emission of TAMRA among the three dendrimer generations at higher polymer concentrations more prominently, the corresponding individual spectrum of $D_{FT}$ was normalized at 521 nm in the emission maxima of fluorescein (Figure 6, right panel). From Figure 6 (right panel) it is clearly evident that initial addition of the polymer does not change the fluorescence intensity of TAMRA with respect to the corresponding fluorescence intensity of fluorescein irrespective of difference in generations. On the other hand, an obvious increase in the fluorescence intensity of TAMRA with respect to fluorescein intensity was seen in Figure 6 (right panel) at higher polymer concentration. More interestingly, the observed raise in the acceptor fluorescence intensity increases with increase in the polymer generation (G1, G2 and G3) especially at higher concentrations. At higher concentration, for every addition of polymer, the observed increase in the acceptor fluorescence intensity with respect to the donor was found to be very huge for G2 (Figure 6b, right panel) and G3 (Figure 6c, right panel) compared to G1 (Figure 6a, right panel). As per our earlier findings, [33] such typical behavior of TAMRA in dual tagged oligonucleic acid ($D_{FT}$) reveals an absence of energy transfer from donor to acceptor up to initial polymer additions. In contrast after certain levels of polymer concentration, a reduction in either inter or intramolecular distance between the donor as well as the acceptor is expected, due to which there is a resonance energy transfer between fluorescein and TAMRA. Further, the observed obvious differences in the acceptor fluorescence energy emission for PAMAM dendrimer of generation one (G1), two (G2) and three (G3) might be attributed to the difference in the packing of the 14 mer in the DNA-dendrimer complex. It is to be noted that eventhough G and C unit adjacent to the following probe molecules, 5'-Fluorescein and 5'-TAMRA respectively are fluorescence quenchers but quenching effect of these base units of the short oligonucleotide are not observed to be interfering with the FRET results.

For a detail understanding of the oligonucleotide-dendrimer interactions, observations from fluorescence and FRET investigations (Figure 5, and 6) are further portrayed as typical

fluorometric titration curves of duplexes $D_F$ (Figure 7, left panel), $D_T$ (Figure 7, left panel) and $D_{FT}$ (Figure 7, right panel) with the dendrimer of required generation. In Figure 7 (left panel), normalized fluorescence intensity maxima of the duplex $D_F$ in the presence of the PAMAM dendrimer of generation one (G1) (Figure 7a, left panel)/ two (G2) (Figure 7b, left panel)/three (G3) (Figure 7c, left panel) ($I_{521}/I^0_{521,}$ where $I_{521}$ and $I^0_{521}$ are oligonucleotide fluorescence intensities in the presence and absence of the dendrimer of required generation) were plotted as a function of $Z_{\pm}$ (dendrimer to the duplex charge ratio). Additionally, Figure 7 (left panel) also portrays normalised fluorescence intensity ($I_{580}/I^0_{580,}$ where $I_{580}$ and $I^0_{580}$ are oligonucleotide fluorescence intensities in the presence and absence of the dendrimer of required generation) of the duplex $D_T$ as a function of dendrimer to $D_T$ charge ratio ($Z_{\pm}$). Figure 7a (left panel) reveals existence of two steps in the complex formation between the duplex $D_F$ and the PAMAM dendrimer of generation one (G1) by showing two breaks at $Z_{\pm} = 0.28$ ($Z^1_{\pm}$) and $Z_{\pm} = 0.55$ ($Z^2_{\pm}$) in the fluorometric titration curve respectively. It is worth mentioning that the other titration curve correspond to $D_T$-G1 system also show two breaks at $Z^1_{\pm}= 0.29$ and $Z^2_{\pm} = 0.5$ further confirming two steps involved in the complexation and the charge ratio values corresponding to two breaks ($Z^1_{\pm}$ and $Z^2_{\pm}$) for the $D_T$-G1 as well as $D_F$-G1 systems respectively are found to be the same. Similar to the PAMAM dendrimer generation one, the other dendrimer generations G2 and G3 also show two breaks for each duplexes $D_F$ and $D_T$ at similar charge ratios. For example, $D_F$-G2 as well as $D_T$-G2 systems the observed charge ratio values for the break $Z^1_{\pm}$ are 0.11 and 0.1 and $Z^2_{\pm}$ is found at the charge ratio 0.26 for fluorescein as well as 0.25 for TAMRA tagged oligonucleotides respectively. In the presence of G3, for duplexes $D_F$ and $D_T$ the break $Z^1_{\pm}$ exists at 0.096 and 0.095 respectively. Whereas, the break $Z^2_{\pm}$ was seen at the charge ratios 0.18 and 0.12 for $D_F$-G3 as well as $D_T$-G3 systems respectisvely. On a comparative basis, interestingly, these two breaks ($Z^1_{\pm}$ and $Z^2_{\pm}$) indicating two steps in the dendrimer- oligonucleotide complex formation are observed to be almost the same for the duplexes $D_F$ and $D_T$ for all the three dendrimer generations. Further, the charge ratio values corresponding to the breaks $Z^1_{\pm}$ and $Z^2_{\pm}$ decrease with increase in dendrimer generations. For example, for $D_F$-G2 system the first break was observed at 0.11 charge ratio and the second was seen at the charge ratio of 0.26. Interestingly, the charge ratio values of these two breaks $Z^1_{\pm}$ and $Z^2_{\pm}$ were further reduced to 0.07 and 0.2 respectively for the duplex $D_F$ in the presence of G3. Such reduction in the break values

observed for dendrimers of increasing generations indicate existence of difference in their interaction with the oligonucleotide.

For the dual tagged duplex $D_{FT}$ $I_{580}/I_{520}$ (where $I_{580}$ and $I_{520}$ are the values correspond to the fluorescence maxima observed for fluorescein as well as TAMRA for each dendrimer concentration respectively) values are plotted against the polymer to oligonucleotide charge ratio ($Z_{\pm}$) (Figure 7, right panel). These normalised FRET ($I_{580}/I_{520}$) values are extracted from Figure 6 (left panel) for the desired dendrimer generation. In the presence of dendrimer G1, two distinct break points for the fluorometric titration curve of the oligonucleotide tagged with donor as well as acceptor ($D_{FT}$) were seen. It is noteworthy that during the titration with G1 the observed first break point for the dual tagged oligonucleotide ($D_{FT}$) at $Z_{\pm}$ is almost in close agreement with the second break $Z^2_{\pm}$ points of both singly tagged duplexes $D_F$ (Figure 7a, left panel) and $D_T$ (Figure 7a, left panel). As observed in the case of G1, the similarity observed for the first break in the fluorometric titration curves of $D_{FT}$ and the second break $Z^2_{\pm}$ for $D_F$ and $D_T$ is also true in the presence of G2 as well as G3. Hence, hereafter, the first break in the titration curves of $D_{FT}$ is represented as $Z^2_{\pm}$ throughout the text. In the case of G1, after $Z^2_{\pm}$ FRET increased gradually and attained maximum at $Z^3_{\pm}$ and thereafter saturation was seen. The reported FRET increase after $Z^2_{\pm}$ indicates a decrease in distance between the donor fluorescein and the acceptor TAMRA. Further, the FRET maximum found at $Z^3_{\pm}$ is an indicative of the closest possible distance between the donor and acceptor moieties, thereafter which remains unaltered indicating saturation at the titration curve for $D_{FT}$-G1 system. It is also noteworthy that in the presence of G1, the highest FRET was observed even before $Z^2_{\pm}$ i.e. at the charge ratio 0.01 (at the first drop of G1) and thereafter decreases to zero at $Z_{\pm}$ = 0.3. The interesting observation below $Z^2_{\pm}$ indicates the aggregation of the $D_{FT}$ molecules due to their competition for the least number of positive sites available at G1 at the lowest concentration. For $D_{FT}$-G1 system, $Z^2_{\pm}$ and $Z^3_{\pm}$ are observed at 0.49 and 0.69 respectively. It is surprising to observe a raise in FRET for the $D_{FT}$-G2 system from the charge ratio 0.20 ($Z^2_{\pm}$) and attain a huge maximum at $Z_{\pm}$ = 0.34 ($Z^3_{\pm}$) compared to $D_{FT}$- G1 system. Interestingly, the obtained maximum FRET at $Z^3_{\pm}$ = 0.34 for $D_{FT}$ in the presence of dendrimer G2 decreases for further raise in $Z_{\pm}$. In the presence of G3, the duplex $D_{FT}$ also showed similar FRET trend as observed in the case of G2. The raise in FRET for G3 begins at the charge ratio ($Z^2_{\pm}$) at 0.1, attains maximum at $Z_{\pm}$ = 0.25 ($Z^3_{\pm}$) and thereafter

decreases. On a comparative basis, the highest FRET value was observed for the polymer G2 at the charge ratio $Z^3_{\pm} = 0.34$ compared to G3 as well as G1. It is noteworthy that normalized FRET intensity value observed for the oligonucleotides $D_{FT}$ in the presence of G3 (3.16) as well as G2 (3.29) is almost three fold higher than the $D_{FT}$-G1 system (1.06). Such a huge FRET intensity reported in the case of $D_{FT}$- G2 and $D_{FT}$- G3 systems is an indicative of the closest packing of oligonucleotides in the corresponding dendriplexes, where either inter- or intra molecular distance between the donor fluorescein and the acceptor TAMRA are expected to be very close to each other. It is pertinent to mention that unlike long DNAs like ct-DNA and plasmid DNA, the rigid and rod structured 14mer oligonucleotide under investigation is most unlikely to undergo bending as well as coiling during the interaction with the dendrimer due to its shorter chain length. Hence during the neutralization process, the intramolecular FRET is ruled out for these 14mer based dendriplexes. The UV melting data on the oligonucleotide ($D_0$) and PAMAM dendrimer of first three generations (Data not shown) reveal denaturation followed by coiling of the oligonucleotides is highly unlikely in the vicinity of the dendrimer (up to the charge ratio $Z_{\pm} = 1$).

**Dendrimer-DNA interaction mechanism.** The fluorescence and FRET investigations on the 14mer based PAMAM dendriplexes of first three generations reveal various steps involved in the dendriplex formation with increase in the polymer concentration. Based on the findings, a schematic representation of the dendriplex formation at increasing dendrimer concentration is displayed in Figure 8 for the PAMAM dendrimer of first three generations. For generation one, at first step a simple electrostatic complexation takes place between the cationic PAMAM dendrimer and the phosphate back bone of the 14mer oligonucleotide resulting in dendriplex formation. It is pertinent to recall the first break ($Z^1_{\pm}$) in the fluorometric titration curves of $D_F$-G1 as well as $D_T$-G1 systems (Figure 7(a), left panel) represents the neutralization point at the charge ratio 0.33. Interestingly, the resulting lowest FRET at this neutralization point (Figure 7(a) right panel) is an indicative of largest distance between the oligonucleotide molecules and also indirectly suggestive of 1:1 complexation between the 14mer oligonuclotide and the dendrimer molecule. The formation of monomeric 1:1 complexation at the neutralization point is well reported in literature for siRNA-PAMAM system using silico[42] as well as SAXS[43] studies. After the step I, observed sharp decrease in fluorescence intensity above the charge ratio 0.3 in the fluorometric titration curves of $D_F$ as well as $D_T$ (Figure 7(a), left panel) is suggestive for the

existence of a strong hydrophobic environment around these fluorophores. Thus, it can be interpreted that at above the neutralization point ($Z_{\pm}$=0.3), the increase in dendrimer concentration causes an addition of new dendrimer molecules into the neutralized dendriplexes followed by an oligonucleotide induced self-assembly to form micellar aggregates. The micellar aggregation of dendrimer in the vicinity of the 14mer represents the step II in the reported schematic diagram (Figure 8). As the raise in FRET from the second break ($Z^2_{\pm}$) in the fluorometric titration curve of $D_{FT}$ with G1 (Figure 7a, right panel) occurs, it reveals arrangement of the oligonucleotide molecules on the surface of dendrimer aggregates starts from the step II. In the presence of the dendrimer G1, the highest energy transfer observed by FRET experiment reported at the charge ratio 0.6 represents the third step of the 14mer-G1 interaction (Figure 7a, right panel). The obtained FRET profile in the case of $D_{FT}$-G1 system confirms an increase in the number of loosely held dendrimer aggregates with its concentration followed by a tight fusion of these aggregates. Interestingly, a simultaneous accommodation of the oligonucleotide molecules also takes place effectively around these dendrimer aggregates from the step II and ends at the third step. At the third step, the local concentration of the oligonucleotide along each dendrimer aggregation increases in such a way to attain the closest possible end-to-end distance between two oligonucleotide molecules and manifests a marked raise in the energy transfer at $Z^3_{\pm}$ (Figure 7a, right panel). Similar to $D_{FT}$-G1 system, in the presence of dendrimer generation two (G2) and three (G3), step I corresponds to monomeric complexation between a dendrimer molecule and a 14mer molecule at the neutralization charge ratio 0.18 as well as 0.12 respectively. With increase in dendrimer concentration, the aggregation of dendrimer molecules revealed by the second break ($Z^2_{\pm}$) observed at the fluorometric titration curves for $D_F$ as well as $D_T$ (Figure 7, left panel) represents the second step. At the second step, here again the lowest FRET is observed for G2 as well as G3. Most interestingly unlike G1, the highest FRET observed at the only charge ratio 0.33 for G2 and 0.23 for G3 indicates the step III. Further the observation of sharp decrease in FRET intensity after the step III for the systems $D_{FT}$-G2 as well as $D_{FT}$-G3 (Figure 7b and 7c, right panel) reveals that with increase in dendrimer concentration the local concentration of the 14mer around the dendrimer aggregate decreases due to the increase in the number of micellar aggregates. Additionally, larger size of G2 as well as G3 in comparison with G1 further increase the end-to-end distance between two DNA molecules with increase in the concentration consequently, decreasing the FRET between the donor and acceptor.

## 4. CONCLUSION

The molecular mechanism of dendriplex formation between the 14mer oligonucleotide and PAMAM dendrimer is successfully elucidated by the fluorescence and FRET investigations. Based on these experimental data, three steps are identified in the dendriplex formation. First step is the neutralization of the 14mer oligonucleotide by the dendrimer molecule in 1:1 ratio. With increase in dendrimer concentration, the oligonucleotide induced self–assembly of dendrimer is considered as step two. The dendrimer aggregation is expected to grow bigger with further raise in its concentration and followed by a fusion of these loosely held dendrimer aggregates at the final step. On the surface of these compact dendrimer aggregates the rigid rod shaped 14mer oligonucleotides are effectively accommodated with the shortest intermolecular distance. The closest packing of the 14 mer molecules on the dendrimer aggregate surface is evidenced by a striking increase in intermolecular FRET between 5′-fluorescein and 5′-TAMRA molecules. Most interestingly, the highest FRET resulted at the aggregates of second generation polymer molecules reveal effective oligonucleotide packing in the dendriplex depends on the dendrimer architecture. Additionally, the observed decrease in the FRET intensities in $D_{FT}$-G2 as well as $D_{FT}$-G3 system confirm that there exist a critical dendrimer to oligonucleotide charge ratio for effective dendrimer packing into the dendriplex.

## ACKNOWLEDGEMENT

Financial support for this work (DST fast track project SR/FT/CS-77/2010) from the Department of Science and Technology, Government of India, New Delhi, is gratefully acknowledged. Authors thank Dr. Souvik Maiti and his co-workers from Institute of Genomics and integrative Biology (CSIR), Mathura Road, Delhi-110 025, India for the experimental support.

## REFERENCES

1. L. Aagaard, J. J. Rossi, *Adv. Drugs Deliver. Rev.,* 2007, **59**, 75–86.
2. I. Sifuentes-Romero, S. L. Milton, A. Garcia-Gasca, *Mutat. Res.,* 2011, **728**,158–171.
3. C. C. Mello, D. Jr. Conte, *Nature,* 2004, **431**, 338–342.
4. A. de Fougerolles, H. P. Vornlocher, J. Maraganore, J. Lieberman, *Nat. Rev. Drug Discov.,* 2007, **6**, 443–453.

5. R. S. Christopher, YiqiSeow, J. A. Wood Matthew, *Mol Ther.,* 2010, **18**, 466-476.
6. Scott M. Hammond, A. Amy Caudy, J. Gregory Hannon, *Nat. Rev. Genet.,* 2001, **2**,110-119.
7. A. Potti, R. L. Schilsky, J. R. Nevins, *Sci. Transl. Med.,* 2010, **2**, 28-13.
8. J. Nguyen, F. C. Szoka, *Acc. Chem. Res.,* 2012, **45**, 1153–1162.
9. D. J. Gary, N. Puri, Y.Y. Won, *J. Control. Release,* 2007, **121**, 64–73.
10. H. Shen, T. Sun, M. Ferrari, *Cancer Gene Ther.,* 2012, **19**, 367–373.
11. S. Nimesh, N. Gupta, R. Chandra, *J. Biomed. Nanotechnol.,* 2011, **7**, 504–520.
12. I. Posadas, F.J. Guerra, V. Cena, *Nanomedicine,* 2010, **5**, 1219–1236.
13. Y. Gao, L. X. Liu, X. R. Li, *Int. J. Nanomed.,* 2011, **6**, 1017–1025.
14. M. Jafari, M. Soltani, S. Naahidi, D. N. Karunaratne, P. Chen, *Curr. Med. Chem.,* 2012, **19**, 197–208.
15. R. S. Dias, B. Lindman, Eds. John Wiley and Sons: Hoboken. NJ., 2008.
16. C. Dufes, I. F. Uchegbu, A. G. Schatzlein, *Adv. Drug Deliv. Rev.,* 2005, **57**, 2177–2202.
17. Y. Gao, G. Gao, Y. He, T. Liu, R. Qi, *Mini Rev. Med. Chem.,* 2008, **8**, 889–900.
18. S. Biswas, P. Vladimir Torchilin, *Pharmaceuticals,* 2013, **6**, 161-183.
19. D. G. Shcharbin, B. Klajnert, M. Bryszewska, *Biochemistry (Moscow),* 2009, **74**, 1070-1079.
20. K. Wada, H. Arima, T. Tsutsumi, Y. Chihara, K. Hattori, F. Hirayama, K. Uekama, *J. Control. Release,* 2005, **104**, 397-413.
21. R. Q. Huang, Y. H. Qu, W. L. Ke, J. H. Zhu, Y. Y. Pei, C. Jiang, *FASEB J.,* 2007*,* **21**, 1117-1125.
22. M. L. Ainalem, R. A. Campbell, S. Khalid, R. J. Gillams, A. R. Rennie and T. Nylander, *J. Phys. Chem. B,* 2010, **114**, 7229–7244.
23. S. Monteagudo, F. C. PérezMartínez, M. D. Pérez-Carrión, J. Guerra, S. Merino, M. P. Sánchez-Verdú and V. Ceña, *Nanomedicine*, 2012, **7(4)**, 493–506.
24. Y. Yang, S. Sunoqrot, C. Stowell, J. Ji, C. W. Lee, J. W. Kim, S. A. Khan and S. Hong, *Biomacromolecules,* 2012, **13**, 2154−2162.
25. K. Fant, E. K. Esbjo¨rner, P. Lincoln, B. Norde´n, *Biochemistry,* 2008, **47**, 1732-1740.
26. E. Vuorimaa, A. Urtti, R. Seppa¨nen, H. Lemmetyinen and M. Yliperttula, *J. Am. Chem. Soc*., 2008, **130**, 11695–11700.

27. O. Taratula, O. B. Garbuzenko, P. Kirkpatric, P. Pandya, I. R. Savla, V. P. Pozharov, H. He, T. Minko, *J. Control. Release,* 2009, **140**, 284–293.
28. S. Spagnou, A. D. Miller, M. Keller, *Biochemistry,* 2004, **43**, 13348–13356.
29. D. J. Gary, N. Puri, Y. Y. Won, *J. Control. Release,* 2007, **121**, 64–73.
30. L. B. Jensen, G. M. Pavan, M. R. Kasimova, S. Rutherford, A. Danani, H. M. Nielsen, C. Foged, *Int. J. Pharm.,* 2011, **416***,* 410–418.
31. S. X. Cheng, Z. Jiehua, L. Xiaoxuan, W. Jiangyu, Q. Fanqi, Z. Zhi-Ling, P. D. Wen, Q. Gilles, Z. Cheng-Cai and P. Ling, *Org. Biomol. Chem.,* 2007, **5**, 3674–3681.
32. A. P. Perez, E. L. Romero, M. J. Morilla, *Int. J. Pharm.,* 2009, **380**, 189-200.
33. D. Santhiya, S. Maiti, *J. Phys. Chem. B,* 2010, **114**, 7602-7608**.**
34. D. A. Tomalia, J. B. Christensen, U. Boas, *Cambridge University Press*, 2012, 29-33.
35. L. A. Marky, K. S. Blumenfeld, S. Kozlowski, K. Breslauer, *J. Biopolym.,* 1983, **22**, 1247-1257.
36. H. Kaur, A. Arora, J. Wengel, S. Maiti, *Biochemistry,* 2006, **45**, 7347-7355.
37. M. J. Waring, *J. Mol. Biol.,* 1965, **13**, 269-282.
38. M. Fried, D. M. *Nucleic Acids Res*., 1981, **9**, 6505-6525.
39. V. M. Jadhav, R. Valaske, S. Maiti, *J. Phys. Chem. B,* 2008, **112***,* 8824−8831.
40. J. B. LePecq, C. Paoletti, *J. Mol. Biol*., 1967, **27**, 87-106.
41. B. Armitage, C. Yu, C. Devadoss, G. B. Schuster, *J. Am. Chem. Soc*., 1994, **116**, 9847-9859.
42. G. M. Pavan, L. Albertazzi, A. Danani, *J. Phys. Chem. B,* 2010, **114**, 2667–2675.
43. L. B. Jensen, K. Mortensen, G. M. Pavan, M. R. Kasimova, D. K. Jensen, V. Gadzhyeva, H. M. Nielsen, C. Foged, *Biomacromolecules,* 2010, **11**, 3571–3477.

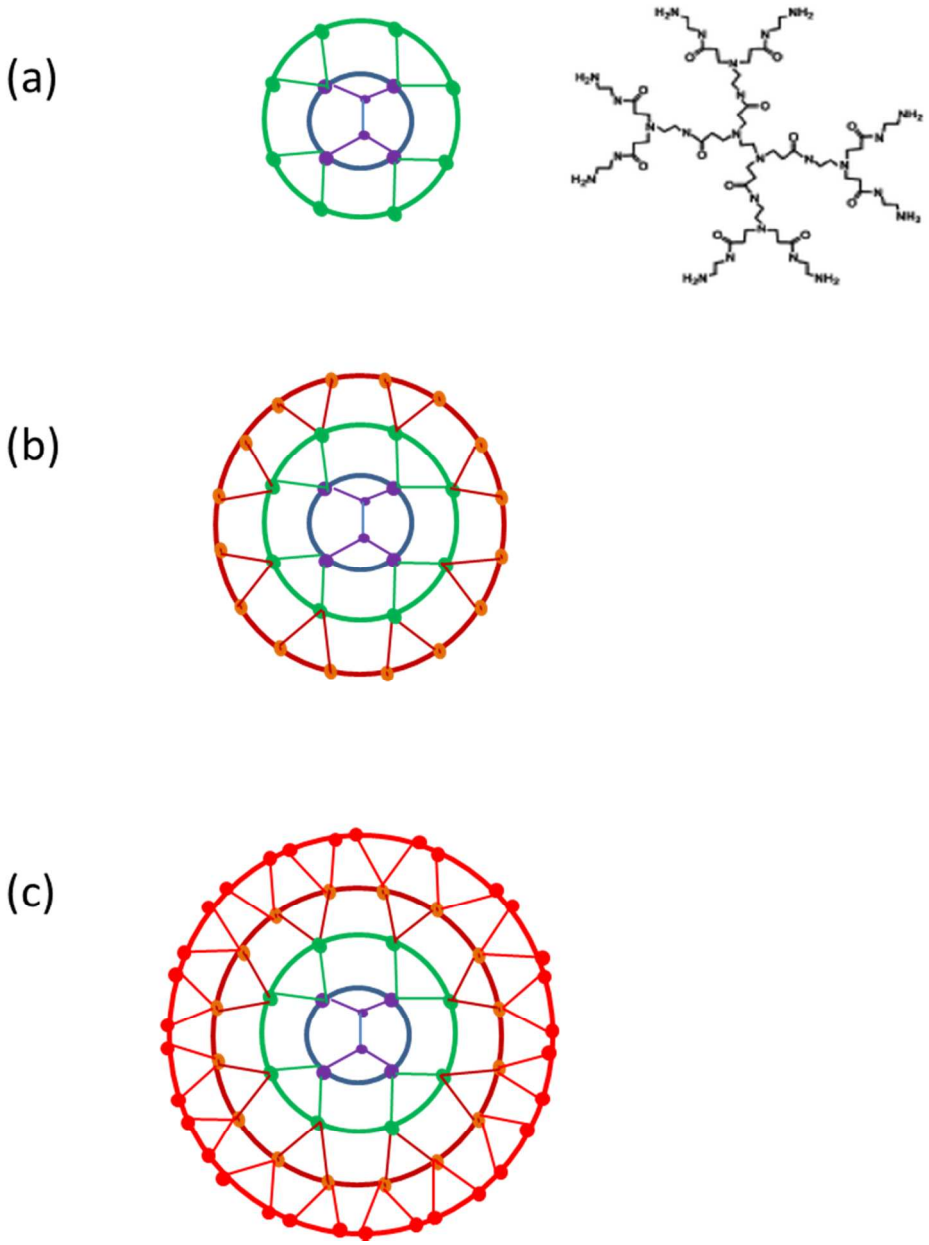


**Figure 1 Chemical structure of poly (amidoamine) (PAMAM) dendrimer of Generation 1 (G1) and Schematic representation of first three PAMAM dendrimer generations (a) G1, (b) G2 and (c) G3. Color Code: Purple: Core; Green: Generation 1; Brown: Generation 2; Red: Generation 3.**

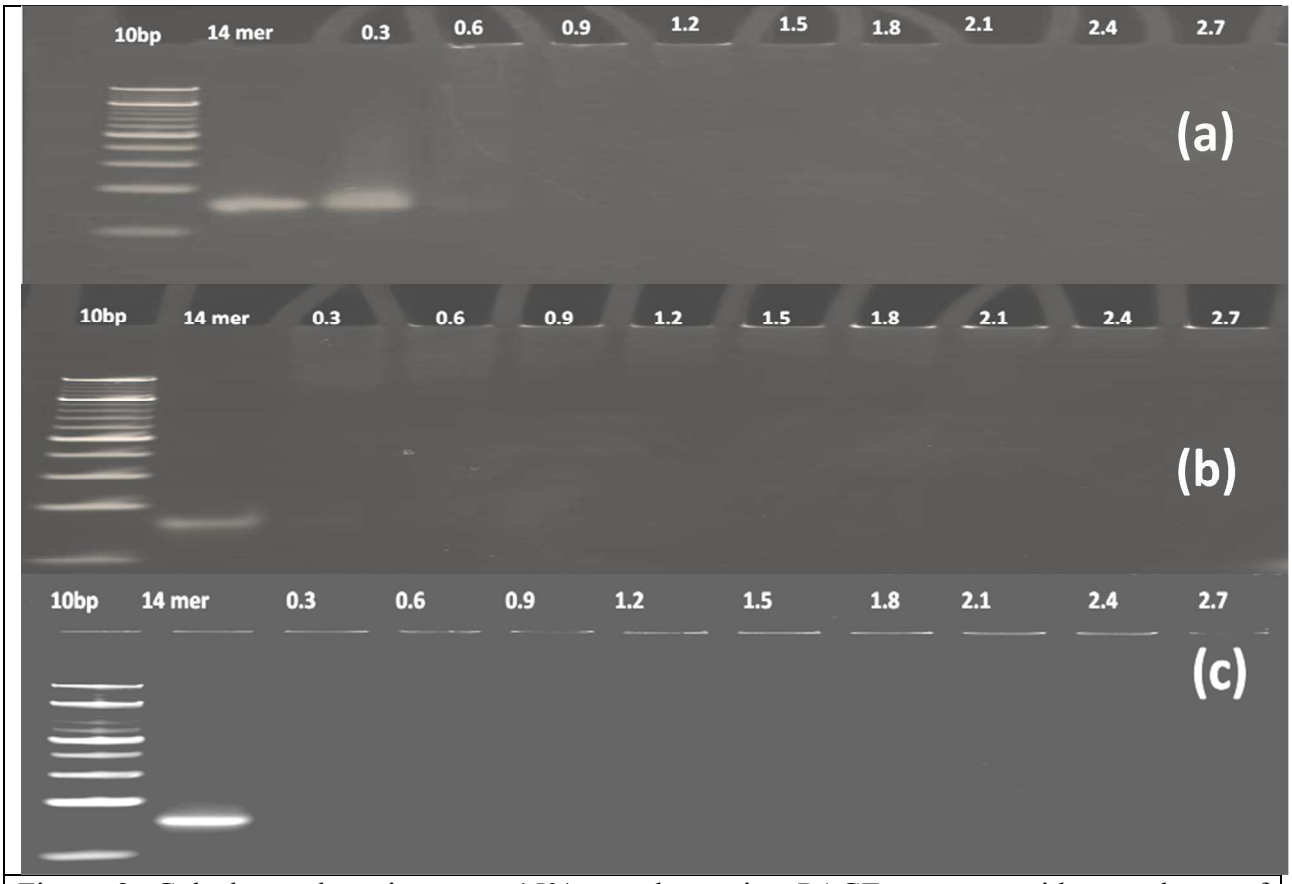


Figure 2. Gel electrophoresis assay. 15% non-denaturing PAGE was run with complexes of PAMAM dendrimer (a) G1 (b) G2 and (c) G3 at various PAMAM dendrimer to oligonucleotide charge ratios (as mentioned on the corresponding lanes). The gel was run in buffer consisting of 45 mM Tris-borate and 1 mM EDTA at pH 8.0, at 120 V for 60 min at 4°C. The gels were visualized under UV illumination after staining with ethidium bromide at room temperature.

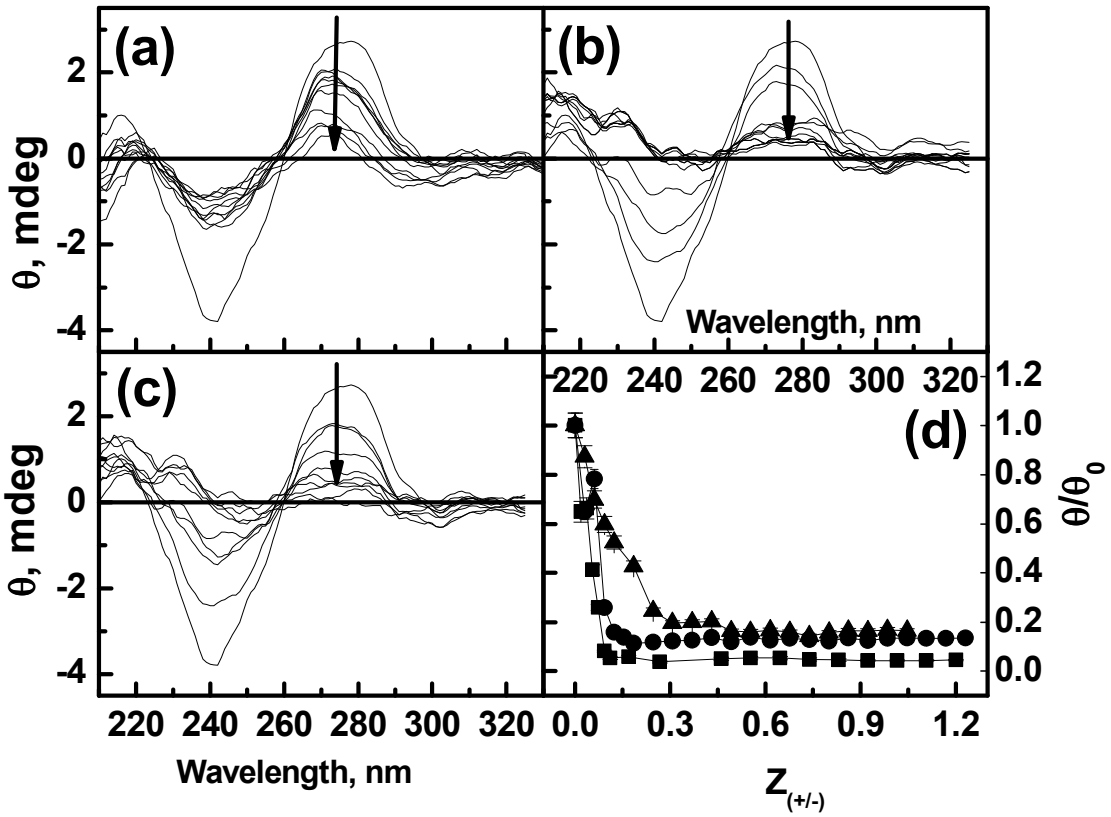


Figure 3: CD spectra of oligonucleotides in the presence of varying amounts of PAMAM dendrimers of (a) generation 1 (G1), (b) generation 2 (G2), (c) generation 3 (G3), and (d) $\theta/\theta_0$ vs $Z_{(+/-)}$ plot for PAMAM dendrimers of various generations G1 ( ▲), G2 (●) and G3 ( ■) in 10 mM sodium phosphate buffer (pH 7.0). The oligonucleotide concentration was 5 μM in 10 mM sodium phosphate buffer.

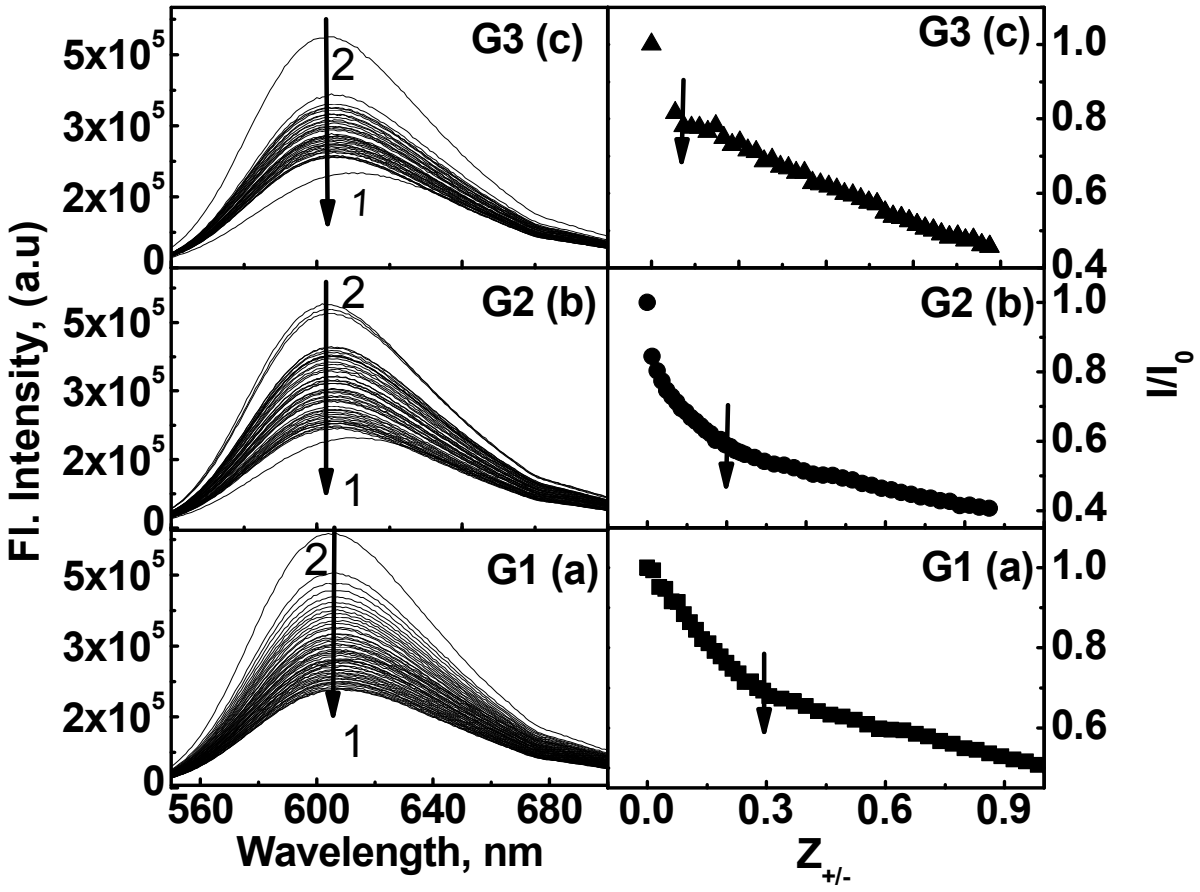


Figure 4. EB exclusion experiments for PAMAM dendrimer (a) G1, (b) G2, and (c) G3. Left panels are emission spectra. The down arrows indicate the increment of $Z_{+/-}$. Right panels are $I/I_0$ vs $Z_{+/-}$ plots. The oligonucleotide concentration was 1 μM in 10 mM sodium phosphate buffer (pH 7.0).

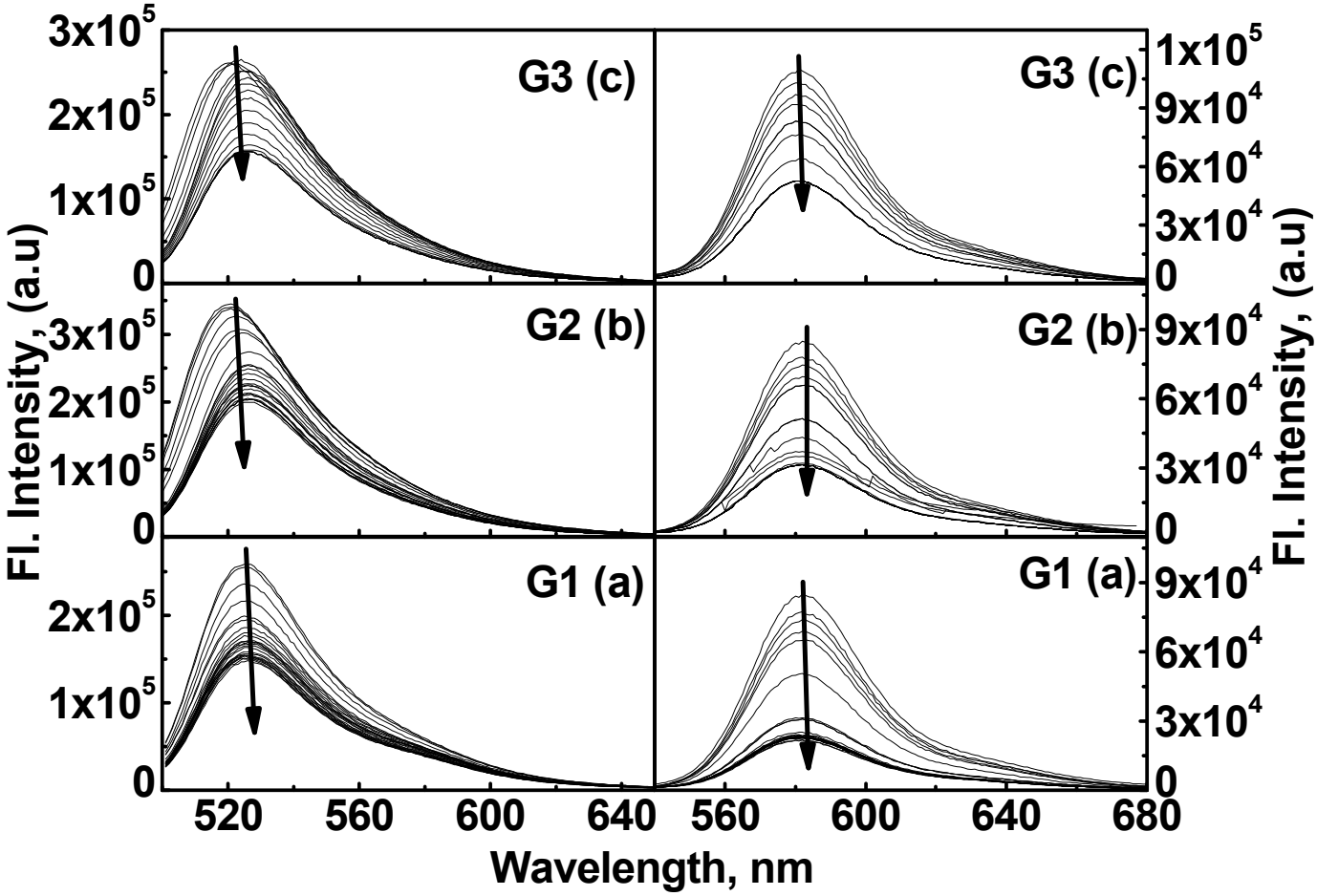


Figure 5. Fluorescence emission spectra of oligonucleotide in the left panel $D_F$ (5′-fluorescein labeled) and right panel $D_T$ (5′-TAMRA labeled) in the absence and presence of increasing concentrations of PAMAM dendrimer (a) G1 (b) G2 and (c) G3. The oligonucleotide concentration was 1 μM in 10 mM sodium phosphate buffer (pH 7.0). The increment of $Z_{+/-}$ is indicated by arrow heads.

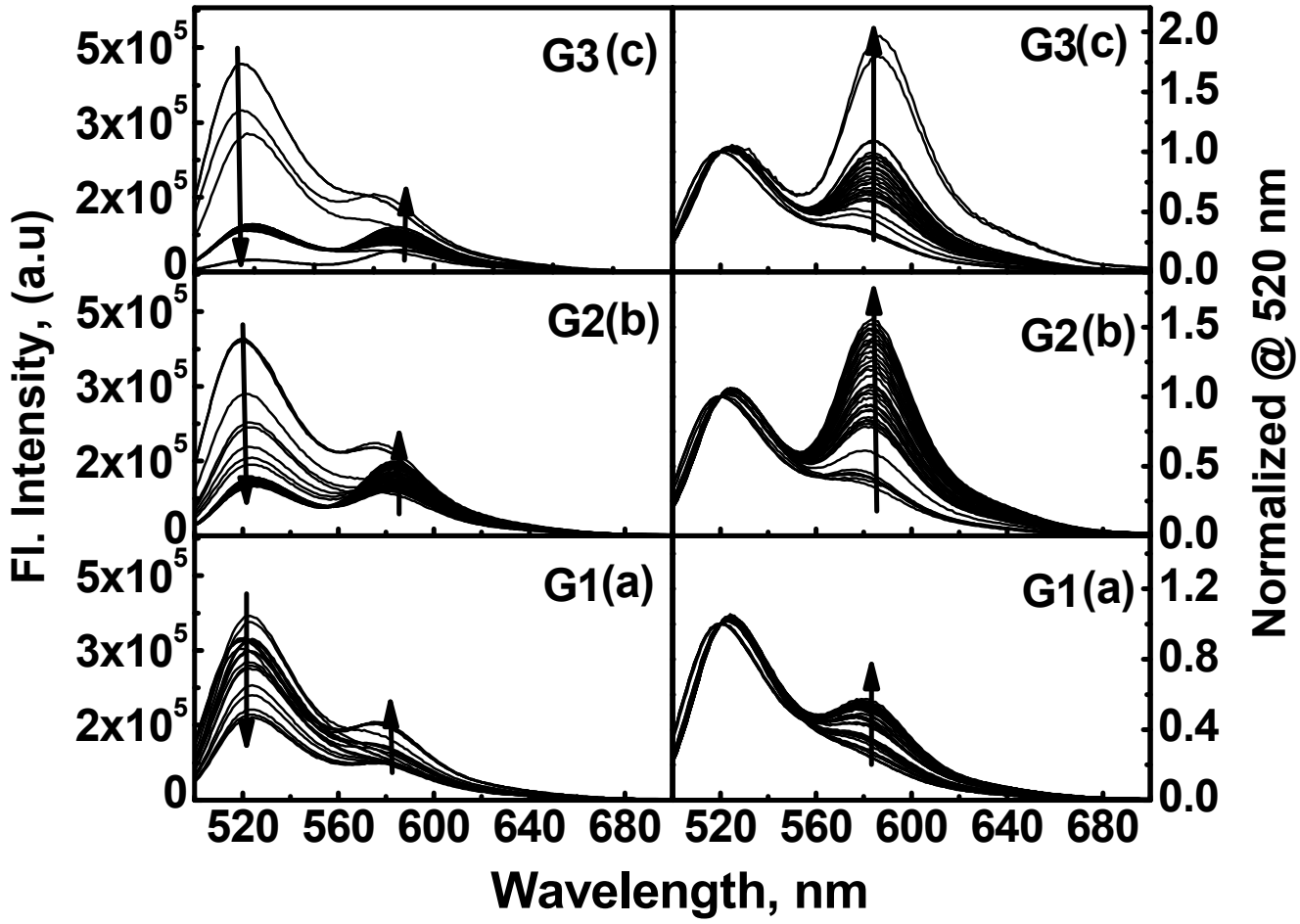


Figure 6. Fluorescence emission spectra of the oligonucleotide in the left panel $D_{FT}$ (5′-fluorescein and 5'- TAMRA labeled) and right panel normalized spectra at 520 nm in the absence and presence of increasing concentrations of PAMAM dendrimer (a) G1, (b) G2 and (c) G3. The oligonucleotide concentration was 1 μM in 10 mM sodium phosphate buffer (pH 7.0). The increment of $Z_{+/-}$ is indicated by arrow heads.

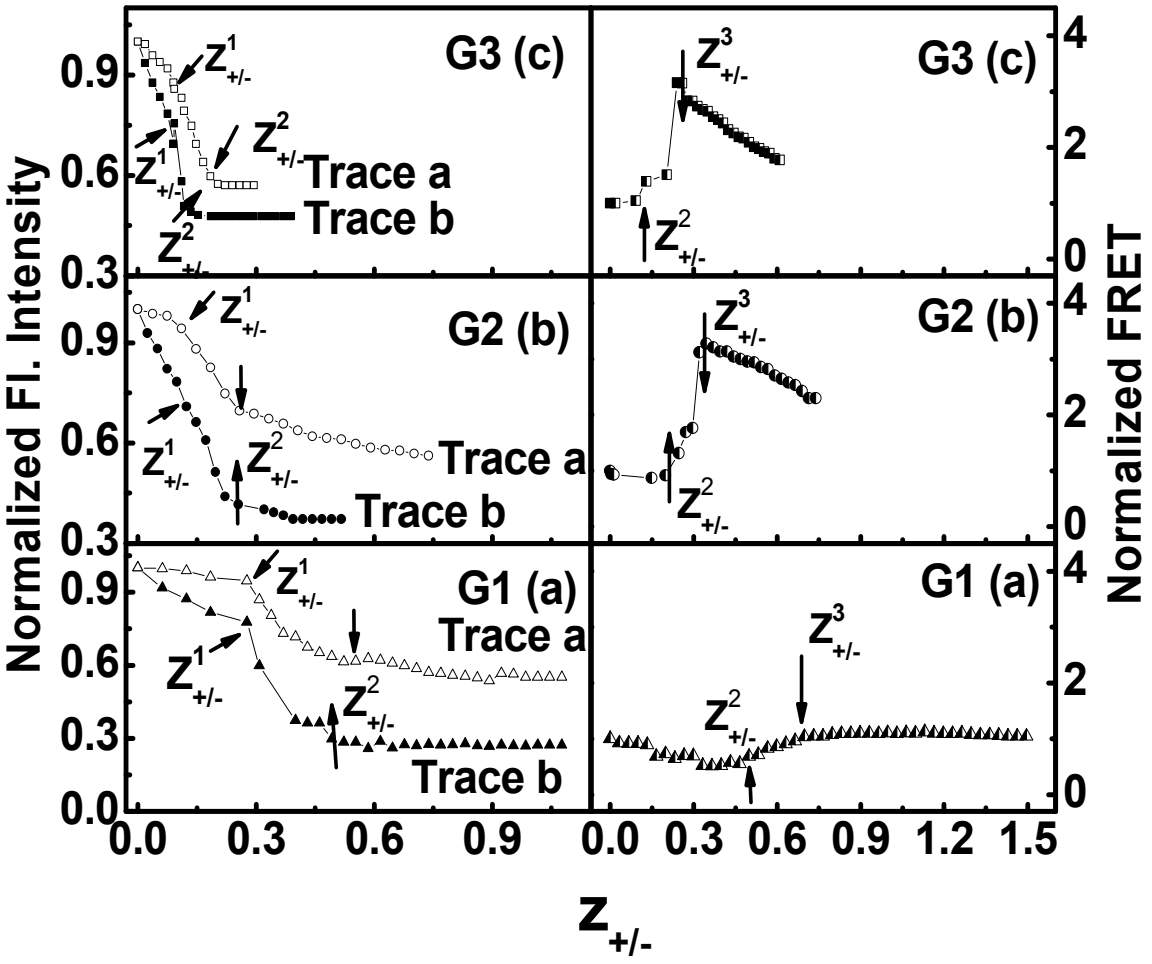


Figure 7. Fluorometric titration curves of the oligonucleotides in the left panel; the above traces are $D_F$ (5′-fluorescein labeled) & below traces are $D_T$ (5′-TAMRA labeled) and the traces of $D_{FT}$ (5′-fluorescein and 5′-TAMRA labeled) are shown in the right panel in the absence and presence of increasing concentrations of PAMAM dendrimer (a) G1, (b) G2 and (c) G3 to oligonucleotide charge ratios. The oligonucleotide concentration was 1 μM in 10 mM sodium phosphate buffer (pH 7.0). Break points $Z^1_{+/-}$, $Z^2_{+/-}$ and $Z^3_{+/-}$ are represented by arrows.

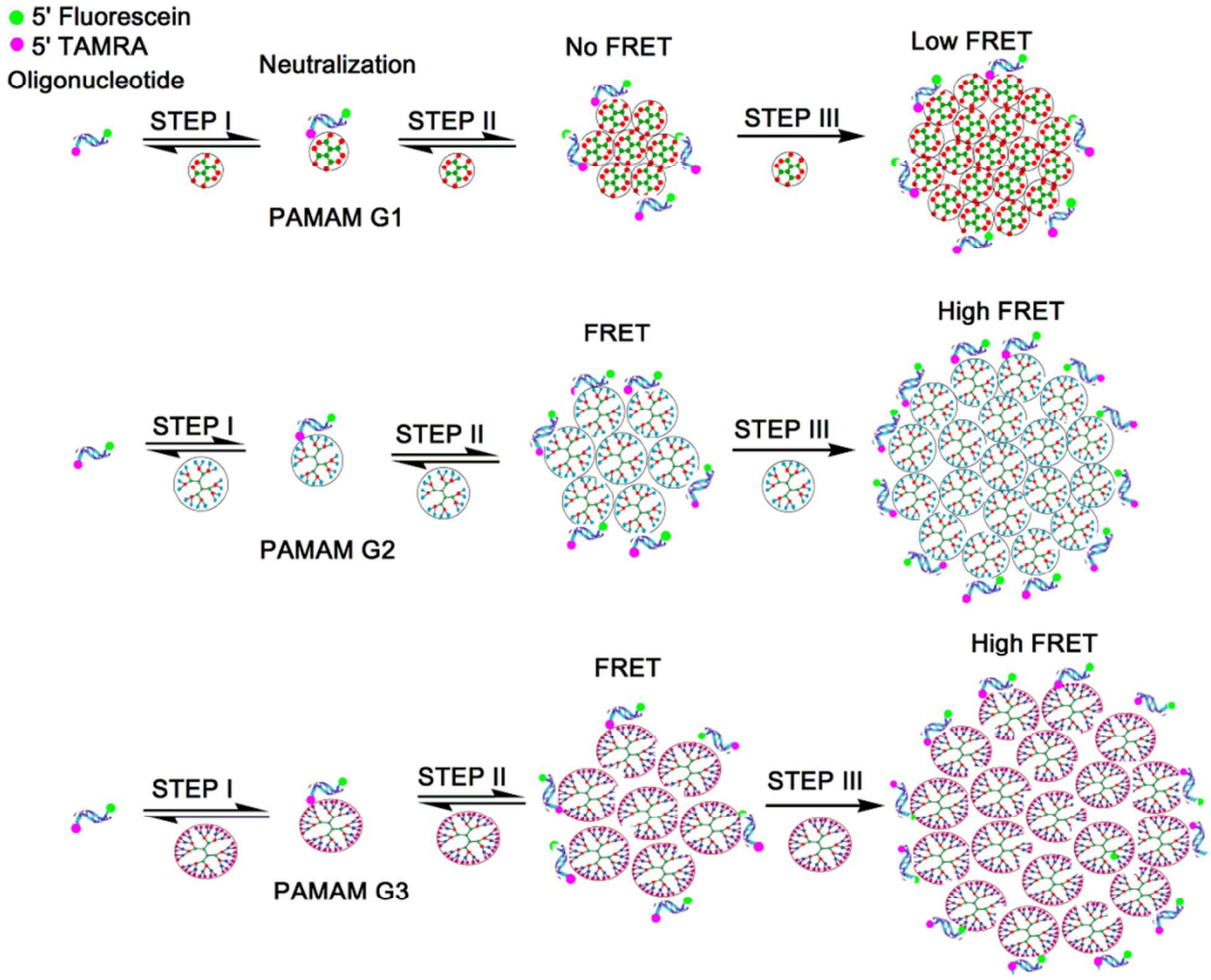


Figure 8. Schematic representation of PAMAM dendrimer and oligonucleotide interaction for G1, G2 and G3.